JOURNAL OF MATERIALS SCIENCE **37** (2002) 3965 – 3972

Experimental verification of the effects of friction and residual stress on the analysis of interfacial debonding and toughness in single fiber composites

BEN W. KIM*
Structural Design & Development Branch, Air Vehicle Directorate,
Air Force Research Laboratory, Wright-Patterson Air Force Base, Ohio 45433-7531, USA
E-mail: Ben.Kim@wpafb.af.mil

JOHN A. NAIRN
Department of Materials Science & Engineering, University of Utah,
Salt Lake City, Utah 84112, USA

Single-fiber fragmentation tests were done on AS4 carbon fiber/epoxy and E-glass/epoxy specimens. Using a new interpretation of the photoelasticity fringes around fiber breaks we measured debonds that occurred instantaneously after each fiber break. The new techniques led to measured debond lengths that were longer than in prior studies. An energy balance analysis of the debond size when the breaks are far apart was used to investigate the interfacial fracture toughness. The best analysis was one that accounted for both residual stress effects and interfacial friction. It was not possible to determine all effects by debonding experiments alone and thus the most accurate results for interfacial toughness require supplemental experiments such as Raman spectroscopy or additional fragmentation observations. The best estimate for interfacial toughness was 220 J/m^2 for carbon-fiber/epoxy and 120 J/m^2 for glass-fiber/epoxy.

---

1. Introduction

In the single-fiber fragmentation test [1–13], a single fiber is embedded in a matrix and loaded in tension. As the load increases, the fiber experiences multiple fractures. Initially, the fiber breaks are isolated and random. As loading continues, the breaks begin to interact and eventually reach a saturation state in which the fiber breaks stop. The average fragment length at saturation is known as the critical fragment length. Various models of the fragmentation test have used critical fragment length results to deduce information on interfacial properties such as interfacial shear strength [1]. But, fiber fracture is not the only fracture process that occurs during single-fiber fragmentation tests. In glass-fiber composites, optical observations show that interfacial debonds occur. In fact every fiber break is accompanied by a finite amount of fiber/matrix debonding that occurs simultaneously with each fiber break [6–10]. In carbon-fiber composites, Raman spectroscopy similarly confirms that all new fiber breaks are associated with fiber/matrix debonding [11, 12]. With careful photoelasticity methods, debonds in carbon-fiber specimens can also be observed optically [13].

Clearly the amount of interfacial debonding must be related to the interfacial fracture toughness. It was therefore proposed that observations of instantaneous debonding associated with each fiber break can be used to measure interfacial toughness [6]. Two advantages of this approach are that experimental results can be derived from each fiber break, rather than just relying on saturation critical fragment length, and that interfacial fracture toughness is probably a more fundamental failure property than interfacial shear strength [14]. The basic approach to interpreting instantaneous debonds is to consider the fiber breaks and instantaneous debond growth as the fundamental fracture event in a fragmentation test. Using energy balance, it is then assumed the total energy released by the fiber fracture and debond growth (total energy released) is equal to the energy required to break the fiber and form the debonds (energy absorbed). The experiments measure debond size as a function of applied load and current fragment length. The modeling calculates the total energy released during each fracture event and thus it is possible to deduce the total energy absorbed. The total energy absorbed is a combination of fiber fracture toughness (Γ_f) and interfacial or debonding fracture toughness (Γ_d). For

---

*Author to whom all correspondence should be addressed.

glass-fiber and carbon-fiber composites, it can be expected that the fiber fracture toughness is very low ($\Gamma_f \ll \Gamma_d$) and thus the analysis mostly gives information on debonding toughness.

There are two regimes in the single-fiber fragmentation test. Initially, the fiber breaks are isolated and the fiber fragments are long—the long-fiber limit. In this limit, the mechanics analysis is greatly simplified because the modeling can be simplified to an isolated fiber break for a fiber embedded in an infinite amount of matrix. Furthermore, the experiments are simplified because it has been observed that all debonding is confined to the instantaneous debonding that occurs immediately after the initial fiber break. In other words, continued loading causes new fiber breaks with debonds, but no propagation of prior debonds [13]. As fiber fracture continues, the fiber breaks begin to interact. Although it is possible to continue analysis in this regime [15], the mechanics analysis is complicated by fiber break interactions. It is also more complicated experimentally because it has been observed that prior debonds begin to propagate [13].

This paper is confined to experiments and analysis in the long-fiber limit. This regime was originally analyzed by a simplified energy balance that ignored residual stresses and friction on the debond surfaces [7]. It is clear, however, that residual stresses are present in glass-fiber and carbon-fiber composites due to differential thermal shrinkage that occurs from processing temperature down to room temperature [16, 17]. Raman spectroscopy has also confirmed that debond surfaces are not stress free but probably have frictional effects [11, 12]. In an energy analysis of the microbond tests, it was shown that inclusion of residual stresses and friction is vitally important for a correct evaluation of interfacial fracture toughness [18]. When these effects are ignored, the analysis leads to the wrong toughness, even if that analysis agrees well with experiments. Only by correct inclusion of residual stress and friction effects is it possible to determine the *true* debonding toughness. We describe new experiments for instantaneous debonds in glass-fiber and carbon-fiber composites in the long fiber limit. These results were analyzed by a recent energy balance analysis that includes both friction and residual stresses [19]. The experiments were also analyzed by models that ignore friction [15] or ignore both friction and residual stresses [7]. The interpretation of the experiments was profoundly affected by analysis method. We claim that an analysis that includes friction and residual stresses is needed to get the *true* debonding toughness. Unfortunately, due to experimental scatter and to the form of the models, it was not possible to distinguish the analyses by how well they fit the data. In other words, observations of debond size in the long-fiber limit alone are insufficient for unambiguous determination of debonding toughness. These observations have to be supplemented by separate experiments that can measure the magnitude of the residual stress and friction effects. Two possible supplementary experiments are Raman spectroscopy [11, 12] or continued debond observation into the saturation regime [13, 15].

2. Experimental

All debonding experiments were done using the single-fiber fragmentation test specimens. All specimens used a transparent matrix which enabled observation of the fragmentation process with an optical microscope. When photoelasticity is added to the optical microscopy by using crossed polarizers, the distribution of stresses can be observed around the fiber breaks. Such photoelastic analyses are a good way to study the stress fields around a single fiber embedded in a birefringent matrix. The fragmentation tests here investigated initial debonds and debonding growth at each fiber break with increasing strain. The experimental work has been done using E-glass and AS4-carbon fiber composites. Those fibers were embedded as single fibers in each specimen. More details on the experimental procedure of the single fiber fragmentation test are given in Ref. [13]. The test apparatus is shown in Fig. 1.

2.1. Specimen materials

Epoxy resins are commonly used in composites because they adhere well to many fillers, reinforcing agents, or substrates, and do not release any volatiles or water during curing. Thus, the shrinkage after curing is usually lower than with other resins. They also have resistance to chemicals and provide good electrical insulation. The epoxy resin used in these experiments was *Shell Epon Resin 828* that includes Diglycidyl Ether of Bisphenol A (DGEBA). The epoxy group can bond chemically with other materials such as curing agents. The curing agent used here was *m*-Phenylenediamine (*m*-PDA). The fibers used were AS4 carbon fibers and E-glass fibers. Details on single-fiber specimen molding and preparation are given in Ref. [13].

2.2. Debond growth observation

To measure debond lengths, the specimens were observed using photoelasticity while under load. Some typical results for a single fiber break are shown in Fig. 2. The size of the measured debond zones are also shown. As explained Ref. [13], the location of the

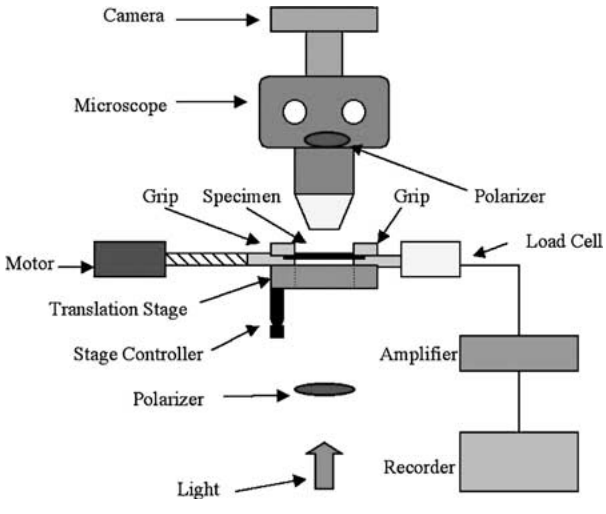

Figure 1 A schematic diagram of the fragmentation test apparatus.

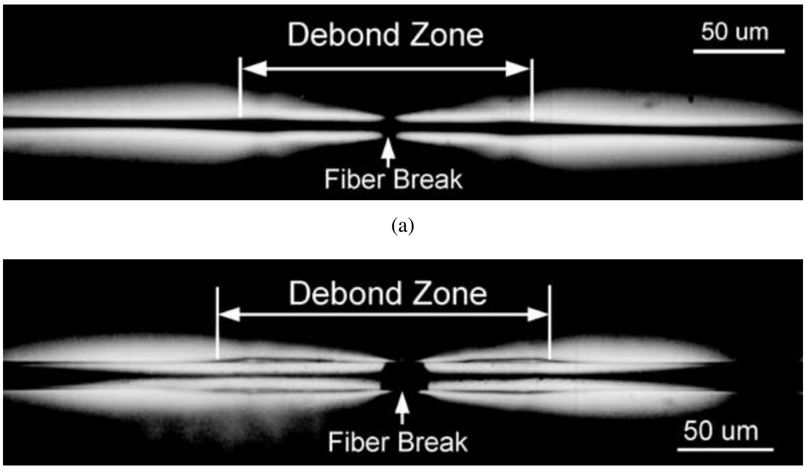

(a)

(b)

Figure 2 Typical photoelastic fringe patterns at fiber breaks in fragmentation tests. (a) AS4-carbon fiber in an epoxy matrix. (b) E-glass fiber in an epoxy matrix.

debond tip was determined by careful observation of the photoelasticity fringes. The debond tip could be observed as a clear photoelasticity effect very close to the fiber surface. This effect does not show up well in the figure, but was easy to detect by visual inspection. The length of the debonds in the typical results in Fig. 2 is indicated. Another way to estimate the debond tip is to note that the photoelasticity effect arises from differences in principal stress which also imply magnitude of the maximum shear stress. Stress analysis of a perfectly bonded fiber always shows that the maximum shear stress is very close to the fiber end [20]. Thus, if there was no debonding the maximum width of the photoelasticity patterns should be very near the fiber break. In all experiments, however, the photoelasticity effect was a minimum at the fiber break, gradually increased to a maximum, and then decreased again far from the fiber break. A similar behavior for shear stresses follows from stress analysis that includes debonding [12]. These analyses further show that the maximum shear stress is always close to the debond tip [12]. In other words, another method to locate the debond tip is to find the location for the maximum width of the photoelasticity effect. The debond tip should be slightly closer to the fiber break than the the maximum photoelasticity effect. The similarity between this approach and our direct observations supports our claim that the effect actually observed does identify the debond tip.

Note that there is a large black zone around the fiber break in E-glass specimens. We previously assumed this effect is due to fiber slippage [13]. This assumption has been confirmed by recent Raman experiments [21]. Some researchers have identified this "opaque" zone as an observation of fiber/matrix debonding. We claim actual debonding extends much farther along the fibers than this zone. A similar opaque zone does not appear in carbon fiber specimens because the fibers themselves are opaque. We expect that carbon-fiber slippage does occur, but that it can not be observed optical.

3. Energy balance for interfacial debonding

An energy balance analysis to predict debonding following a fiber break treats fiber fracture and instantaneous debonding as a fracture event. It is then assumed that the energy released by the fiber fracture and debond growth is balanced by the *effective* surface energy required to create the new fiber break and the observed amount of debonding [6]. In the long-fiber limit, it suffices to consider an isolated fiber break in a fiber embedded in a large amount of matrix. The energy balance then becomes [19]

$$\begin{aligned}\pi r_f^2 \Delta G_{f\infty} + 2\int_0^{L_d/2} 2\pi r_f G_{d\infty}(x)\,\mathrm{d}x \\ = \pi r_f^2 \Gamma_f + 2\pi r_f L_d \Gamma_d \end{aligned} \quad (1)$$

where $\Delta G_{f\infty}$ is the energy release rate for formation of an isolated fiber break, $G_{d\infty}(x)$ is the energy release rate for growth of a debond of length x at an isolated debond, L_d is the final debond length (growth of $L_d/2$ on either side of the fiber break), and r_f is the fiber radius. The terms Γ_f and Γ_d or the fiber fracture toughness and the interfacial fracture toughness. The subscript ∞ on the energy release rates emphasizes that this analysis is in the long-fragment limit or for an isolated fiber break.

By applying this energy balance to a finite fracture mechanics analysis of debonding with very few assumptions, Nairn [19] was able to derive a good starting point for energy balance analysis from Equation 1 to be:

$$\begin{aligned}\Gamma_d = \frac{r_f \psi_\infty^2}{4E_A}\left(1 - \frac{\psi_f L_d}{r_f} + \frac{\psi_f^2 L_d^2}{3r_f^2}\right) \\ + \frac{r_f \Delta G_{f\infty}}{2L_d}\left(1 - \frac{\psi_f L_d}{2r_f}\right)\left(1 - \frac{\psi_f L_d}{r_f}\right) - \frac{\Gamma_f r_f}{2L_d}\end{aligned} \quad (2)$$

where ψ_∞ is the far-field stress on the fibers (both applied stress and residual stress), E_A is the axial modulus of the fibers, and ψ_f is an *effective* friction coefficient. Friction is introduced by assuming there is a constant shear stress on the debond fracture surfaces. A rigorous analysis of friction would relate this shear stress to the interfacial normal stresses. Experimental results, however, only give axial stress. In a linear elastic analysis, the radial stress must be linearly related to the applied loads. If friction is linearly related to normal stresses through a true friction coefficient, then it can also be linearly related to axial load through an *effective* friction coefficient:

$$\tau_{friction} = \mu\sigma_{rr} = \mu\,(k\psi_\infty) = \psi_f\psi_\infty \qquad (3)$$

All calculations here are done in terms of this *effective* friction coefficient, ψ_f. The far-field stress can be related to applied axial stress and temperature differential by analysis of an unbroken fiber in an infinite matrix [20]:

$$\psi_\infty = \frac{\left(\frac{2\nu_A\nu_m}{E_A} - \frac{1-\nu_T}{E_T} - \frac{1+\nu_m}{E_m}\right)\frac{E_A\sigma_0}{E_m} + \left(\frac{2\nu_A}{E_A}(\alpha_T-\alpha_m) + \left(\frac{1-\nu_T}{E_T} + \frac{1+\nu_m}{E_m}\right)(\alpha_A-\alpha_m)\right)E_A\Delta T}{\frac{2\nu_A^2}{E_A} - \frac{1-\nu_T}{E_T} - \frac{1+\nu_m}{E_m}} \qquad (4)$$

where E_A, E_T, ν_A, ν_T, α_A, and α_T are the axial and transverse moduli, Poisson's ratios, and thermal expansion coefficients of the fiber, and E_m, ν_m, and α_m are the modulus, Poisson's ratio, and thermal expansion coefficient of the matrix. σ_0 is the total applied load applied to the specimen and $\Delta T = T_s - T_0$ is the temperature differential between the specimen temperature (T_s) and the stress-free temperature (T_0).

Equation 2 is nearly exact, within the assumption of constant friction stress, but it is incomplete. It is written in terms of the energy release rate for an isolated fiber break, $\Delta G_{f\infty}$. This term needs to be derived to complete the analysis. Here we choose to write $\Delta G_{f\infty}$ in terms or a new dimensionless parameter, β, as:

$$\Delta G_{f\infty} = \frac{r_f\psi_\infty^2}{\beta E_A} \qquad (5)$$

Equation 2 can then be rewritten as

$$\Gamma_d = \frac{r_f\psi_\infty^2}{12E_A}\left[1 + \left(1 - \frac{\psi_f L_d}{r_f}\right)\left(2 - \frac{\psi_f L_d}{r_f}\right) \times \left(1 + \frac{3r_f}{\beta L_d}\right)\right] - \frac{\Gamma_f r_f}{2L_d} \qquad (6)$$

This equation gives the full analysis which allows one to calculate interfacial toughness for any observations of debond length. The analysis requires input information for applied load, σ_0, and thermal effect, ΔT, which are needed to find ψ_∞, prior knowledge of the friction effect, ψ_f, and the fracture toughness of the fibers, Γ_f, and an evaluation for the parameter β. If the fiber fracture toughness is small, the second terms will be insignificant compared to the first and debonding toughness can be found without knowledge of Γ_f.

Two special cases for Equation 6 are when one ignores friction or ignores both friction and residual stresses. When friction is ignored, $\psi_f = 0$ and Equation 6 reduces to

$$\Gamma_d = \frac{r_f\psi_\infty^2}{4E_A}\left[1 + \frac{2r_f}{\beta L_d}\right] - \frac{\Gamma_f r_f}{2L_d} \qquad (7)$$

This result matches a previous frictionless result in Ref. [15] (note that Ref. [15] had Q instead of 1 for the first term in the parentheses, but $Q \approx 1$ for most conditions). A result that ignores both friction and stresses can be obtained simply by calculating ψ_∞ needed for Equation 7 using $\Delta T = 0$. Another result in the literature, however, that ignores friction and residual stresses is

$$\Gamma_d = \frac{r_f\sigma_f^2}{4E_A}\left[1 + \frac{2r_f}{L_d}\left(\frac{1}{\beta_{cox}} - \frac{\beta_{cox}E_A}{16G_A}\right)\right] - \frac{\Gamma_f r_f}{2L_d} \qquad (8)$$

which identical to Equation 7 except total fiber stress ψ_∞ is replaced by fiber stress σ_f that ignores residual stresses and β is replaced by

$$\beta = \frac{\beta_{cox}}{1 - \frac{\beta_{cox}^2 E_A}{16G_A}} \qquad (9)$$

In this prior analysis β_{cox} was the shear-lag parameter derived by Cox [22:]

$$\beta_{cox}^2 = \sqrt{\frac{4G_m}{E_A \ln\frac{1}{V_f}}} \qquad (10)$$

where G_m is the shear modulus of the matrix and V_f is the *effective* volume fraction of the fiber in the matrix.

For the calculations in this paper, we analyzed experiment results for L_d as a function of ψ_∞ where ψ_∞ was calculated from fiber and matrix properties, the applied stress, and a ΔT term estimated from material thermal properties. We assumed $\Gamma_f = 10$ J/m^2, although, because it is small, any small number, even zero, would give similar results. We tried various values for *effective* friction coefficient. The remaining unknown is β or equivalently, the energy release rate for fiber fracture alone. The form for $\Delta G_{f\infty}$ in Equation 5, was chosen because it is also the form used in recent shear lag models for calculation of energy release rate due to an fiber fracture [14, 15]. In shear-lag analysis, β is the shear-lag parameter, although it was found that the shear-lag parameter proposed by Cox [22] is very inaccurate. The optimal shear lag parameter [14] is the one derived instead by Nayfeh [23] and given by

$$\beta^2 = \frac{2}{E_A E_m} \times \left[\frac{E_A V_f + E_m(1 - V_f)}{\frac{1 - V_f}{4G_A} + \frac{1}{2G_m}\left(\frac{1}{1 - V_f}\ln\frac{1}{V_f} - \frac{3 - V_f}{2}\right)} \right] \quad (11)$$

where G_A is the axial shear modulus of the fibers.

A problem with all shear-lag models, including both the inaccurate Cox analysis [22] and an optimal shear-lag analysis [14] based on the Nayfeh parameter [23], is that they depend on an *effective* fiber volume fraction, V_f. A typical approach in shear-lag models for the fragmentation test is simply to make an *ad hoc* assumption about V_f, but it is possible to do better. There are two alternatives to arbitrary assumptions. First, shear-lag analysis can be *calibrated* by comparison to more advanced methods that do not need assumptions about effective fiber volume fraction. Two examples are Bessel-Fourier series methods [20], or finite element analysis [14]. If $\Delta G_{f\infty}$ can be found by some other means, the shear lag parameter can be found from

$$\beta = \frac{r_f \psi_\infty^2}{\Delta G_{f\infty} E_A} \quad (12)$$

Once β is found, Equation (11) can be used to determine the *effective* fiber volume fraction. Second, because β in a shear-lag analysis relates to the rate of stress transfer from the fiber to the matrix, β can be measured by comparison of Raman results for stress transfer [12] to a shear-lag analysis for stress transfer [15]. For the analyses in this paper, we used the first approach. By comparison to Bessel-Fourier series analysis for carbon-epoxy and glass-epoxy specimens we determined $V_f \approx 0.16\%$. In prior shear-lag models, it is common to quote a ratio R/r_f which is a ratio of the zone of matrix influenced by the fiber, R, to the fiber radius, r_f. The effective volume fraction of $V_f \approx 0.16\%$ corresponds to a ratio $R/r_f = 25$.

4. Results and discussion

The carbon-epoxy and glass-epoxy single-fiber specimens were loaded in tension until the fiber started to fracture. Soon after the first break, the loading was stopped and each fiber break was examined under the microscope using photoelasticity. Typical photoelastic fringes around a break are shown in Fig. 2. The length of the debond was measured using the methods described in the *Experimental* section. In brief, the debond tip showed up as a distinct photoelastic effect close to the fiber surface. This effect does not show up well in Fig. 2, but it was clear by direct observation. Although most previous optical methods have been on glass-epoxy specimens, it was possible here to locate debond tips in both carbon-epoxy and glass-epoxy specimens. The fact that we located the correct debond tip was confirmed both by theoretical arguments (see *Experimental* section) and by additional experiments on some specimens (see Ref. [13]). In addition to debond lengths, we also mapped the entire damage pattern. Finally the average debond length was recorded corresponding to the axial load currently on the specimen.

After the first observation, the loading was continued to higher loads. The loading was periodically stopped. Each time it was stopped, we mapped the new damage state and measured th lengths of all debond zones. By comparing the damage map at any particular load to the previous damage map, it was possible to determine which fiber breaks had formed during the most recent loading interval. We averaged the debond length of only the new fiber breaks. All results in this paper plot the average of the new debonds as a function of applied axial load. For each fiber type we ran several experiments. For a single specimen, the debond lengths increased monotonically with load. The scatter in the plots was a result of sample-to-sample variations. All debond lengths were normalized to fiber diameter (L_d/r_f) and thus give the debond aspect ratio.

Figs 3–5 show the results for carbon-epoxy specimens analyzed by ignoring residual stresses and friction (Equation 8), by including residual stress, but ignoring friction (Equation 7) and by including both residual stresses and various levels of friction (Equation 6). The fitting was done by solving each equation for ψ_∞ and then fitting results for ψ_∞ as a function of L_d at constant Γ_d. For all calculations, we used $\Gamma_f = 10$ J/m^2. This fiber toughness was derived from literature results [24], but as long as the correct value is small, it has little effect on the data analysis. The shear-lag parameters (β and β_{cox}) were derived from the fiber and matrix properties in Table I using an *effective* fiber volume fraction of $V_f = 0.16\%$ ($R/r_f = 25$). For residual stress calculations, we assumed $\Delta T = -100^\circ$C, which is equal to the temperature difference between the final cure temperature (125°C) and room temperature (25°C).

Within scatter of the experimental data, all equations can fit the data equally well, but the end result for

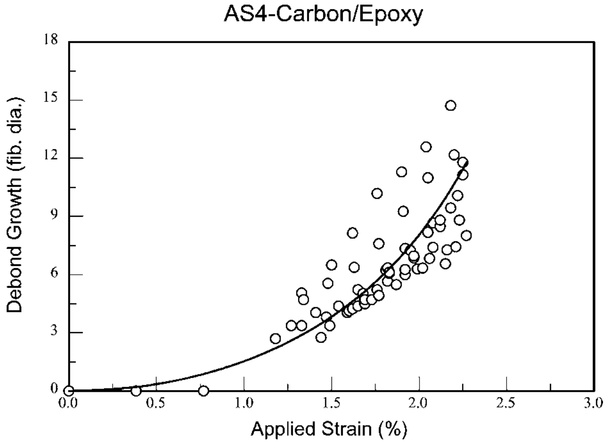

Figure 3 Aspect ratio of the average debond length at new fiber breaks as a function of the applied strain for AS4-carbon fibers in an epoxy matrix. The experiments were analyzed using Equation 8 which ignores both residual stresses and friction.

TABLE I Mechanical and thermal properties use the in the analyses for the AS4-Carbon and E-Glass fibers and the epoxy matrix

Property	AS4-Carbon	E-Glass	Epoxy
Diameter (r_f in μm)	7	14	
Axial modulus (E_A or E_m in MPa)	231	72.5	2.6
Transverse modulus (E_T or E_m in MPa)	40	72.5	2.6
Axial shear modulus (G_A or G_m in MPa)	20	27.9	0.97
Transverse shear modulus (G_T or G_m in MPa)	16	27.9	0.97
Axial poisson's ratio (ν_A or ν_m)	0.2	0.3	0.34
Transverse poisson's ratio (ν_T or ν_m)	0.25	0.3	0.34
Axial thermal expansion (α_A or α_m in ppm/K)	−0.7	5.4	40
Transverse thermal expansion (α_T or α_m in ppm/K)	10	5.4	40

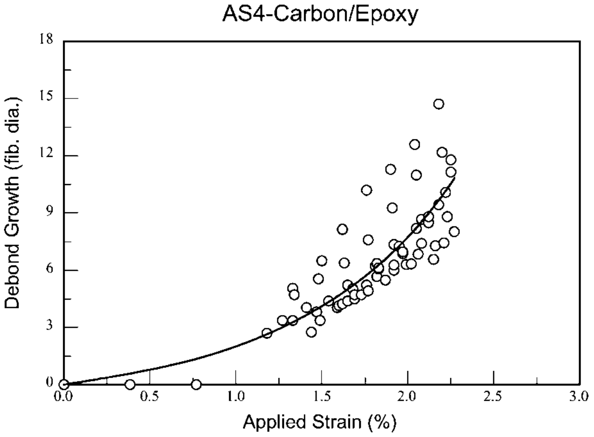

Figure 4 Aspect ratio of the average debond length at new fiber breaks as a function of the applied strain for AS4-carbon fibers in an epoxy matrix. The experiments were analyzed using Equation 7 which includes residual stresses (using $\Delta T = -100°\text{C}$), but ignore friction.

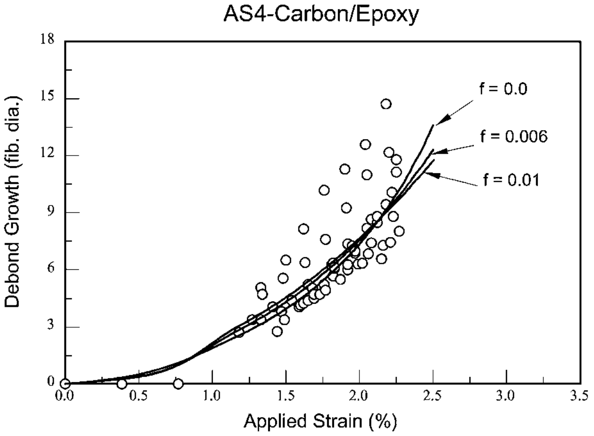

Figure 5 Aspect ratio of the average debond length at new fiber breaks as a function of the applied strain for AS4-carbon fibers in an epoxy matrix. The experiments were analyzed using Equation 6 which includes residual stresses (using $\Delta T = -100°\text{C}$) and various levels of friction ($\psi_f = 0$, $\psi_f = 0.006$ and $\psi_f = 0.01$).

debonding toughness is strongly influenced by analysis method. The best fit when ignoring residual stresses and friction was $\Gamma_d = 283$ J/m^2. When the analysis includes residual stresses, the best-fit toughness increased to $\Gamma_d = 367$ J/m^2. There are two reasons for the difference. First, the residual stresses put the fiber in compression and thus for a given applied stress of σ_0, the value of ψ_∞ is lower when residual stresses are included then when they are ignored. By this reason, the toughness would have to be decreased to fit the same experimental results because the applied load is actually supplying less energy to the fiber break [18]. The second reason is that Equation 8 uses the Cox shear-lag parameter while Equation 7 uses the optimal shear lag parameter. The Cox parameter gives a result that significantly underestimates the toughness. Combining these two reasons, the end result is that the analysis that included residual stresses using Equation 7 gave a higher toughness than the analysis using Equation 8. If Equation 7 was used in an analysis that ignored residual stresses, thus having the residual stress effect without the shear-lag parameter effect, the calculated Γ_d would be higher than 367 J/m^2.

The results for an analysis that includes both friction and residual stresses depends on the amount of friction. Fig. 5 shows three analyses for $\psi_f = 0$, $\psi_f = 0.006$, and $\psi_f = 0.01$. It was not possible to determine the amount of friction by judging the quality of fit. If the friction coefficient got too high, however, the fit curve start to curve downward and eventually gave poor fits. We selected $\psi_f = 0.006$ and a representative analysis with friction. Compared to the analysis that included only residual stress, the toughness from an analysis that includes both friction and residual stresses was significantly lower—$\Gamma_d = 220$ J/m^2. When friction is included, some of the energy released is used in frictional work and thus less is available for debonding. As a result, the calculated toughness is lower [18].

The experimental results and analysis for glass-epoxy specimens are given in Figs 6–8. The results of fitting to all three equations follow the same pattern as the carbon-epoxy analysis. Using an equation that ignores friction and residual stresses and has an inaccurate shear-lag parameter (Equation 8), the debonding toughness was found to be $\Gamma_d = 201$ J/m^2. Using an improved shear-lag parameter and including residual stresses changes $\Gamma_d = 213$ J/m^2. In other words,

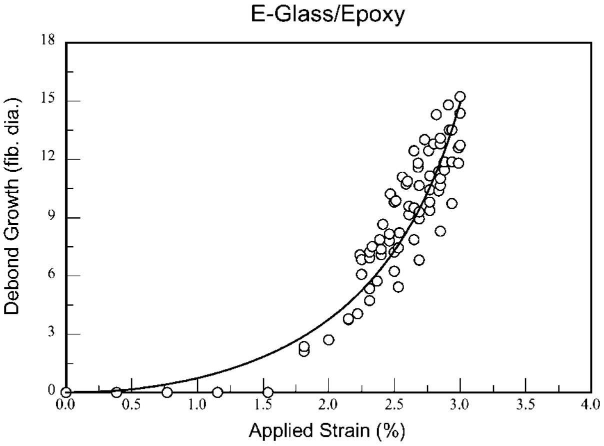

Figure 6 Aspect ratio of the average debond length at new fiber breaks as a function of the applied strain for E-glass fibers in an epoxy matrix. The experiments were analyzed using Equation 8 which ignores both residual stresses and friction.

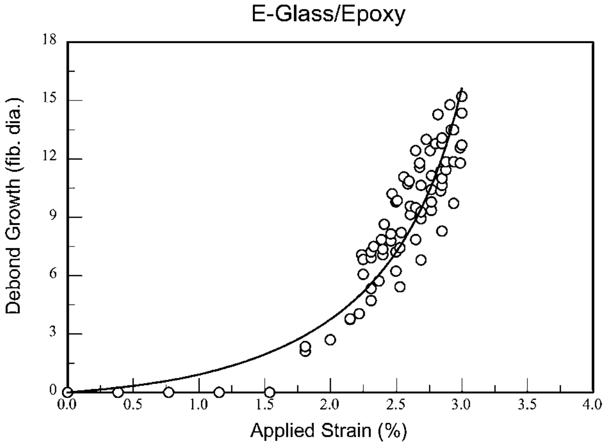

Figure 7 Aspect ratio of the average debond length at new fiber breaks as a function of the applied strain for E-glass fibers in an epoxy matrix. The experiments were analyzed using Equation 7 which includes residual stresses (using $\Delta T = -100°\text{C}$), but ignore friction.

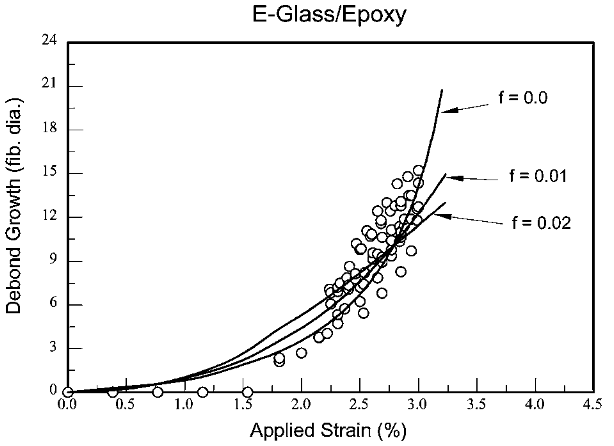

Figure 8 Aspect ratio of the average debond length at new fiber breaks as a function of the applied strain for AS4-carbon fibers in an epoxy matrix. The experiments were analyzed using Equation 6 which includes residual stresses (using $\Delta T = -100°\text{C}$) and various levels of friction ($\psi_f = 0$, $\psi_f = 0.01$ and $\psi_f = 0.02$).

the residual stress effect and the shear-lag parameter effect nearly cancel each other. The analyses that includes friction and various levels of friction are given in Fig. 8. The effect of friction was larger in glass-epoxy than in carbon epoxy laminates and values too low or too high gave poorer fits. We selected $\psi_f = 0.01$ as a represented friction analysis. With this level of friction, the debonding toughness changed to $\Gamma_d = 120$ J/m^2.

The results of all analyses for both carbon-epoxy and glass-epoxy are summarized in Table II. We claim that only an analysis that includes the correct level of residual stresses and friction gives the correct results for debonding toughness. Thus, the experiments should be analyzed by Eq. (6). By this equation, our results for the carbon-epoxy interface was $\Gamma_d = 220$ J/m^2, while the glass-epoxy interface had a lower toughness of $\Gamma_d = 120$ J/m^2. Although the proper analysis includes all real effects present in the system. we could not be certain of the actual level of friction. If subsequent experiments show that the friction stress was different, our result for interfacial toughness would change. If there is no information about friction, an analysis that ignores friction can be used, but that analysis gives an *upper bound* to the *true* toughness.

TABLE II Calculated interfacial debonding toughness using a variety of analysis methods. All shear-lag parameters were calculated with $V_f = 0.16\%$

Specimen	ΔT (K)	ψ_f	Equation	Γ_d(J/m^2)
AS4-carbon/epoxy	0	0	8	283
AS4-carbon/epoxy	−100	0	7	367
AS4-carbon/epoxy	−100	0.006	6	220
E-glass/epoxy	0	0	8	201
E-glass/epoxy	−100	0	7	213
E-glass/epoxy	−100	0.01	6	120

Our findings, therefore, are that observations of instantaneous debonding alone are insufficient for determination of the correct value for interfacial debonding toughness. To get the correct result, debonding experiments need to be combined with other experiments that can measure residual stresses and friction. Two options are to do Raman experiments or to continue debonding experiments to higher loads where the fiber breaks begin to interact. Raman spectroscopy can directly measure residual stresses and frictional shear stress. Preliminary analysis of experiments at higher crack density show that the new debond length reaches a peak and then decreases at very high strain [13, 15]. The decrease at high strain is caused by the fact the fiber breaks release less energy when they begin to interact [20]. Preliminary results further indicate that the magnitude and shape of the peak is strongly influenced by friction [13]. With more debonding data, it is possible that fits alone can uniquely determine both friction coefficient and debonding toughness.

Zhou *et al.* [10] did similar experiments on similar materials and analyzed them by Equation 6 or an alternate equation that includes friction. The alternate equation was based on the methods used to derive Equation 8 but used the optimal shear-lag parameter instead of the Cox shear lag parameter. Their results, however, were very different. The interfacial toughnesses here are about an order of magnitude lower than the results of Zhou *et al.* [10]. There are two differences. First, the two papers used different values for effective fiber volume fraction. Here V_f was estimated to be 0.16% by comparison of shear-lag results to more advanced stress analysis methods. In contrast, Zhou *et al.* [10] estimated V_f to be 0.58%, which was estimated from Raman experiments for stress transfer. Both methods for finding V_f are valid and the V_f values are close enough that they can not account for the differences in toughess. The source of the discrepancy can thus be attributed to the other difference which is the raw experimental results for instantaneous debond length. The debond lengths in Zhou *et al.* [10] were 1–3 fiber diameters for carbon-epoxy specimens and 1–2 for glass-epoxy specimens. In contrast, our debond lengths were 3–12 fiber diameters for carbon-epoxy specimens and 3–15 fiber diameters for glass-epoxy specimens. We claim our new observation of debond lengths is the correct one; this claim is supported by two results. First, the new debond observations places the debond tip close the maximum photoelasticity effect which stress analysis shows should be close to the debond tip. Second, the magnitude of our toughness results appear more realistic for carbon-epoxy and glass-epoxy interfaces. The results in Zhou *et al.* [10] have toughness that exceed that of the matrix. If the interfacial toughness was truly that high, a crack at the interface would instead divert into the matrix and the observed toughness should not exceed the matrix toughness.

5. Conclusion

With careful observations, it was possible to use the photoelasticity effect to locate debond tips in both carbon-epoxy and glass-epoxy specimens. As long as the fiber breaks were isolated, the size of the new debonds increased approximately quadratically with applied axial load. Because all theories follow a quadratic trend, the experimental results could be fit to all analyses that were considered. On physical grounds, however, we argue that theories that ignore real effects, such as residual stresses and friction, will get the wrong result for interfacial debonding toughness. We thus argue that Equation 6 is the proper equation for analysis of instantaneous debonding. It is possible to estimate the residual stresses for single-fiber specimens by thermoelastic analysis of the specimen. It is much more difficult to estimate the magnitude of the friction effect. If Equation 6 is used with residual stresses alone, it will give an upper bound to the *true* interfacial toughness. As the friction effect is introduced, the calculated toughness will decrease as the input amount of friction is increased. The analysis will give the *true* toughness only when the correct amount of friction stress in known. This term can not be calculated from debonding experiments at isolated fiber breaks, but it might be possible to deduce friction from Raman experiments or for additional debonding experiments at higher break density.

Another critical aspect of debond observations is to correctly identify the debond tip. It appears that some prior debonding experiments have underestimated the true debond length. We were able to directly observe longer debond lengths. The actual tip of the debond was always close to the maximum photoelasticity effect. This observation agrees with stress analysis and experimental results for debond zones which shows the maximum interfacial shear stress (and hence maximum photoelasticity effect) is close to the debond tip.

Acknowledgements

This work was supported, in part, by a grant from the Mechanics of Materials program at the National Science Foundation (CMS-9713356).

References

1. A. KELLY and W. R. TYSON, *J. Mech. Phys. Solids* **13** (1965) 329.
2. A. A. FRASER, F. H. ANCKER and A. T. DIBENEDETTO, in Proc. 30th Conf. SPI Reinforced Plastics Div. Section 22-A (1975) p. 1.
3. L. T. DRZAL, M. J. RICH and P. F. LLOYD, *J. Adhesion* **16** (1983) 1.
4. W. D. BASCOM and R. M. JENSEN, *ibid.* **19** (1986) 219.
5. B. YAVIN, H. E. GALLIS, J. SCHERF, A. EITAN and H. D. WAGNER *Polym. Comp.* **12** (1991) 436.
6. H. D. WAGNER and S. LING, *Adv. Comp. Letts.* **2** (1993) 169.
7. H. D. WAGNER, J. A. NAIRN and M. DETASSIS, *Applied Comp. Mater.* **2** (1995) 107.
8. M. DETASSES, E. FRYDMAN, D. VRIELING, X. F. ZHOU, J. A. NAIRN and H. D. WAGNER, *Composites* **27A**(7) (1996) 69.
9. H. D. WAGNER, X.-F. ZHOU and J. A. NAIRN, in First Hellenic Conference on Composite Materials and Structures, Xanthi, Greece, July 2–5 1997.
10. X.-F. ZHOU, J. A. NAIRN and H. D. WAGNER, *Composites* **30** (1999) 1387.
11. N. MELANITIS, C. GALIOTIS, P. L. TETLOW and C. K. L. DAVIES, *J. Comp. Mat.* **26** (1992) 574.
12. A. PAIPETIS, Y. C. LIU, C. GALIOTIS and J. A. NAIRN, *ibid.* **33** (1999) 377.
13. B. W. KIM and J. A. NAIRN, *ibid.*, in press.
14. J. A. NAIRN and Y. C. LIU, *Comp. Interfaces* **4** (1996) 241.
15. J. A. NAIRN and H. D. WAGNER, *Adv. Comp. Letts.* **5** (1996) 131.
16. J. A. NAIRN, *Polym. Comp.* **6** (1985) 123.
17. H. D. WAGNER and J. A. NAIRN, *Comp. Sci. & Tech.* **57** (1997) 1289.
18. C. H. LIU and J. A. NAIRN, *J. Adhes. Adhesives.* **19** (1999) 59.
19. J. A. NAIRN, *Int. J. Fract.* **105** (2000) 243.
20. J. A. NAIRN and Y. C. LIU, *Int. J. Solids Structures* **34** (1997) 1255.
21. T. KISLEV, G. MAROM, L. BERGLUND, R. JOFFE, J. A. NAIRN and H. D. WAGNER, *Adv. Comp. Letts*, in press.
22. H. L. COX, *Brit. J. Appl. Phys.* **3** (1952) 72.
23. A. H. NAYFEH, *Fibre Sci. & Tech.* **10** (1977) 195.
24. B. HARRIS, J. MORLEY and D. C. PHILLIPS, *J. Mater. Sci.* **10** (1975) 2050.

Received 24 April 2001
and accepted 16 May 2002